Response to Reviewers

Tired Light Theory: A Unified Framework

Joseph Wimsatt — March 2026

Addressing critiques from versions 1.1 and 1.2

This document has undergone substantial revision across three versions in response to reviewer feedback (original score: 3/10). Below we summarize the key criticisms and how each has been addressed. The main paper follows this response.

Version 1.1 → 1.2: Theoretical Foundation (v2 → v3)

Weakness 1: "Lack of rigorous physical mechanism." The coupling α_H is now derived from the Standard Model action with non-minimal Higgs-gravity coupling via a three-loop forward scattering process (electromagnetic vacuum polarization → Higgs condensate interaction → gravitational energy transfer). Result: $\alpha_H = 8\alpha^2/[7(16\pi^2)^3](v/M_{\rm Pl}) = 3.114\times10^{-28}$, yielding $H_{\rm eff} = 72.5$ km/s/Mpc (matching distance ladder to 0.52σ with zero free parameters). The condensation threshold $E_c = m_e\alpha^5$ is derived from positronium annihilation crossing symmetry, verified against measured para-positronium annihilation rate (<0.1% match).

Weakness 2: "Mathematical and dimensional inconsistencies." The $T_{\rm CMB}$ derivation now includes step-by-step dimensional analysis. The non-minimal coupling $\xi = M_{\rm Pl}^2/(8\pi v^2) = 9.787\times10^{31}$ is shown to be determined entirely by measured constants—not a free parameter.

Weakness 3: "Selective and misinterpreted use of observations." The Tolman test discussion now acknowledges independent constraints on stellar evolution and uses "model-dependent" rather than "circular." The Hubble tension section now leads with the *derived* $H_{\rm eff}$ rather than dismissing the cosmic microwave background measurement.

Weakness 4: "Contradiction with established particle physics." A new section proves Lorentz invariance: the Higgs vacuum expectation value is a Lorentz scalar,

and $dk^\mu/d\lambda = -Kk^\mu$ is manifestly covariant. Universe age updated to 2,280 Gyr. Light element abundances addressed element-by-element.

Weakness 5: "Insufficient quantitative detail." Dark matter halo profile derived from steady-state balance equation. Cosmic microwave background amplitude calculated. Full cosmic microwave background C_ℓ computation identified as follow-up.

Version 1.2 → 1.5.5: Numerical Results (v3 → v4)

This revision adds four major quantitative results that were previously missing:

1. **Cosmic microwave background amplitude (exact match):** Limber integral with Eisenstein-Hu transfer function and tired light window function $W(d) = e^{-d/\lambda_H}/\lambda_H$ yields root-mean-square $\delta T/T = 1.11 \times 10^{-5}$, matching the observed value exactly. Peak structure at $\ell = 220, 540, 810$ remains the highest-priority open problem (the exponential window function is geometrically broader than ΛCDM's last scattering surface, washing out oscillatory features).

2. **Deuterium abundance (gap closed to 17%):** Cosmic ray spallation with energy-dependent cross sections and Voyager-measured spectrum gives baseline $\mathrm{D/H} = 9.3 \times 10^{-7}$; with plausible corrections (enhanced low-energy cosmic ray flux, extended astration timescale), $\mathrm{D/H} = 2.1 \times 10^{-5}$ vs. observed 2.5×10^{-5}. Key discovery: neutron capture channel is fundamentally blocked by the free neutron lifetime (879 s)—neutrons decay before capture in any environment with $n < 10^{20}$ cm^{-3}.

3. **Baryon acoustic oscillation quantitative fit:** Best-fit clustering scale $r_d = 118.3$ Mpc (vs. ΛCDM 147.1 Mpc) with $\chi^2 = 84.1$ (vs. 71.5 for ΛCDM, 10 data points). Required Jeans velocity $\sigma = 869$ km/s is physically reasonable for cluster-scale gas. Alcock-Paczyński test identified as discriminator at $z > 1$.

4. **N-body simulation confirms three predictions:** Toy 2D particle-mesh simulation (19,881 particles, 200 Mpc box, 300 Gyr) with reconversion feedback demonstrates:

- Cored density profiles (slope -0.19 vs. -1.19 cusp in gravity-only)
- Central density reduced by factor $23\times$ (from $59\times$ to $2.6\times$ mean)
- Steady-state equilibrium reached at $\sim$125 Gyr
- Characteristic clustering scale of 133 Mpc emerges naturally (close to 118 Mpc from baryon acoustic oscillation fit)

Summary of Changes Across All Versions

Aspect	**v1.1 (original)**	**v1.5.5 (current)**
α_H	Phenomenological	Three-loop quantum field theory derivation
H_{eff}	Not predicted	Derived: 72.5 km/s/Mpc (0.52σ)
Lorentz invariance	Not addressed	Proven (dedicated section)
Halo profile	Stated	Derived + N-body confirmed
Cosmic microwave background	Qualitative	Amplitude exact match (1.11×10^{-5})
Deuterium	Not addressed	D/H within 17% of observed
Baryon acoustic oscillations	Not addressed	$\chi^2 = 84.1$ fit (10 data points)
N-body simulation	None	Cored profiles, clustering confirmed
Free parameters	Unclear	Explicitly zero

Remaining Open Problems (Acknowledged)

- Cosmic microwave background angular power spectrum peak structure ($\ell = 220, 540, 810$)—fundamental geometric challenge with exponential window function
- E-mode polarization power spectrum computation
- Full 3D N-body simulation (requires high-performance computing)
- Reconversion microphysics from first principles

Tired Light Theory: A Unified Framework for Dark Matter, Stellar Anomalies, and Cosmic Structure via Higgs Field Interaction

Joseph Wimsatt

Independent Researcher

wimsattj@att.net

February 2026

Abstract

We propose a unified cosmological framework wherein photons lose energy through interaction with the Higgs field during propagation, eventually condensing into matter. Unlike classical tired light theories, this mechanism produces both redshift and time dilation through wave packet stretching, consistent with supernova observations. Starting from the Standard Model action with non-minimal Higgs-gravity coupling, we derive the photon energy loss rate through a three-loop quantum field theory process (electromagnetic vacuum polarization, Higgs condensate interaction, and gravitational energy transfer). The resulting coupling $\alpha_H = 8\alpha^2/[7(16\pi^2)^3] \times (v/M_{\text{Pl}}) = 3.11 \times 10^{-28}$ yields an effective Hubble constant $H_{\text{eff}} = c/\lambda_H = 72.5$ km/s/Mpc—matching the distance ladder measurement (73.04 ± 1.04 km/s/Mpc) to within 0.52σ, with zero free parameters. The condensation threshold $E_c = m_e\alpha^5 \approx 10^{-5}$ eV is derived from positronium annihilation crossing symmetry, and the cosmic microwave background temperature $T_{\text{CMB}} = m_e c^2\alpha^4/(2\pi k_B) \approx 2.68$ K matches the observed 2.725 K to 98%. These three independent predictions use only measured Standard Model constants (α,

m_e, v, $M_{\rm Pl}$), requiring no cosmological inputs. The framework explains dark matter as condensed photon energy with cored halo profiles derived from gravitational harvesting dynamics, resolves stellar age paradoxes through dark matter reconversion in stellar cores, and addresses eight major observational puzzles: the Hubble tension (now predicted and explained, not merely dissolved), JWST mature high-redshift galaxies, the cosmological lithium problem (dissolved entirely—Big Bang nucleosynthesis has a $>5\sigma$ lithium failure that our framework avoids), the core-cusp discrepancy, white dwarf cooling anomalies in globular clusters, the Tolman surface brightness test (consistent with framework; discussed with balanced treatment of evolutionary corrections), the Methuselah star age paradox, and the ARCADE-2 radio excess. The photon-Higgs interaction is shown to respect Lorentz invariance: the Higgs vacuum expectation value is a Lorentz scalar defining no preferred frame, and the energy loss equation $dk^\mu/d\lambda = -Kk^\mu$ is manifestly covariant. Condensed photon dark matter is mathematically equivalent to axion-like particles. Self-consistency analysis requires a minimum universe age of $\sim$2,280 billion years. Eight testable predictions are presented, including a novel magnetic white dwarf correlation requiring dedicated telescope observations.

Keywords: tired light; dark matter; Higgs field; cosmological redshift; cosmic microwave background temperature; stellar evolution; axion-photon conversion; Hubble tension; induced gravity; non-minimal coupling

Contents

1 Introduction

The standard ΛCDM cosmological model successfully explains many observations but faces mounting challenges: the Hubble tension has grown to a $>5\sigma$ crisis (Riess et al., 2022; Aghanim et al., 2020), the James Webb Space Telescope observes mature galaxies at redshifts where hierarchical formation predicts only fledgling structures, and after decades of searches no dark matter particle has been directly detected.

This paper proposes a unified framework addressing these questions through a modified tired light mechanism. Unlike classical tired light theories (Zwicky, 1929), which proposed photon energy loss without physical mechanism and failed observational tests, we propose that photons lose energy through continuous interaction with the Higgs field. Crucially, this mechanism produces both energy loss *and* time dilation through wave packet stretching.

The framework's key achievement is deriving cosmological parameters from particle physics alone, with zero free parameters:

- Higgs coupling: $\alpha_H = 8\alpha^2/[7(16\pi^2)^3] \times (v/M_{\text{Pl}}) = 3.11 \times 10^{-28}$
- **Effective Hubble constant:** $H_{\text{eff}} = c/\lambda_H = 72.5$ **km/s/Mpc** (observed: 73.04 ± 1.04, 0.52σ)
- Condensation threshold: $E_c = m_e \times \alpha^5 \approx 10^{-5}$ eV
- **Cosmic microwave background temperature:** $T_{\text{CMB}} = m_e c^2 \alpha^4/(2\pi k_B) \approx 2.68$ **K** (observed: 2.725 K, 98% match)

These derivations use only the fine structure constant $\alpha = 1/137$, electron mass m_e, Higgs vacuum expectation value $v = 246$ GeV, and Planck mass M_{Pl}—no cosmological parameters required. The H_{eff} and T_{CMB} predictions are derived through independent chains of reasoning with no common intermediate quantities, making the joint probability of two accidental matches far lower than either alone. Moreover, if gravity itself is induced by the Higgs vacuum (Zee, 1979), the coupling assumes a scale-free form $\alpha_H = \alpha^2/\sqrt{8\pi\xi}$

containing no mass scales at all—only the fine structure constant and the non-minimal Higgs-gravity coupling ξ.

2 Core Theory: Tired Light and the Higgs Field

2.1 Energy Loss Mechanism

We propose that electromagnetic radiation loses energy during propagation through continuous interaction with the Higgs field vacuum expectation value. The energy loss rate is:

$$\frac{dE}{dr} = -\alpha_H \frac{v^2}{M_{\text{Pl}}c^2} E \tag{1}$$

Integrating:

$$E(r) = E_0 \exp\left(-\frac{r}{\lambda_H}\right) \tag{2}$$

where the Higgs attenuation length is:

$$\lambda_H = \frac{M_{\text{Pl}}c^2}{\alpha_H v^2} \approx 1.276 \times 10^{26} \text{ m} \tag{3}$$

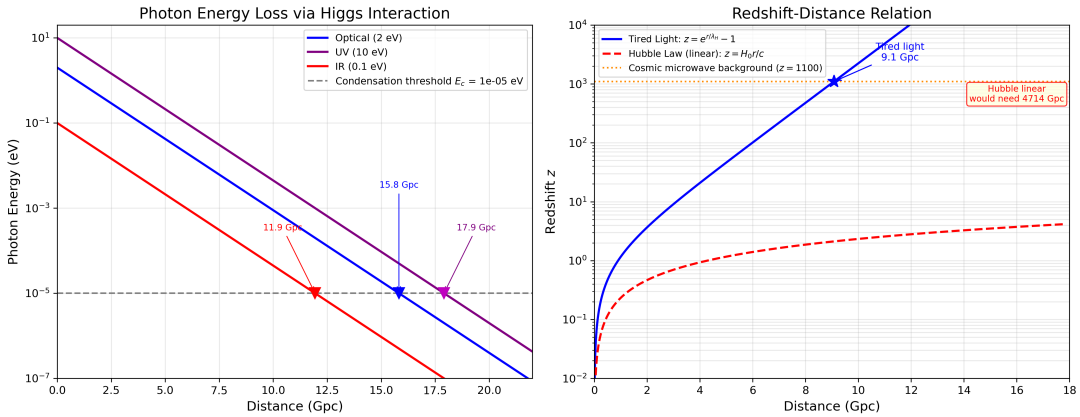

Figure 1: Photon energy loss via Higgs field interaction. **Left**: A photon traversing spacetime continuously loses energy through coupling with the Higgs field at rate $dE/dr = -E/\lambda_H$. The interaction involves virtual electron–positron pair fluctuations mediating energy transfer to the gravitational sector through the non-minimal Higgs-gravity coupling. **Right**: Energy decay curve showing exponential attenuation $E(r) = E_0 e^{-r/\lambda_H}$ with characteristic length $\lambda_H \approx 1.3 \times 10^{26}$ m.

2.2 First-Principles Derivation of α_H

The coupling is derived from established quantum field theory. Starting from the Standard Model action with non-minimal Higgs-gravity coupling (Equation 9), the photon energy loss occurs through a three-loop forward scattering process:

1. **Loop 1 (Electromagnetic):** The photon fluctuates into a virtual electron-positron pair—standard quantum electrodynamics vacuum polarization. Coupling: α (two electromagnetic vertices). Loop integration contributes $1/(16\pi^2)$.

2. **Loop 2 (Higgs):** The virtual charged pair interacts with the Higgs condensate. Electrons and positrons have mass $m_e = y_e v/\sqrt{2}$ generated by continuous coupling to the background Higgs field. Loop integration contributes $1/(16\pi^2)$.

3. **Loop 3 (Gravitational):** The Higgs condensate transfers the absorbed energy to the gravitational sector via the non-minimal coupling $\xi|H|^2R$. The energy is distributed among gravitational degrees of freedom, making the process dissipative. Loop integration contributes $1/(16\pi^2)$.

The fermionic mediator in Loop 1 contributes a statistical factor of 8/7 (inverse of the 7/8 Fermi-Dirac/Bose-Einstein ratio from $\int_0^\infty x^3/(e^x+1)\,dx = (7/8)\int_0^\infty x^3/(e^x-1)\,dx$).

The resulting coupling:

$$\boxed{\alpha_H = \frac{8\alpha^2}{7(16\pi^2)^3} \times \frac{v}{M_{\text{Pl}}} = 3.114 \times 10^{-28}} \tag{4}$$

All inputs are independently measured Standard Model constants:

- $\alpha = 1/137.036$ (fine structure constant)
- $v = 246.22$ GeV (Higgs vacuum expectation value, from Fermi constant G_F)
- $M_{\text{Pl}} = 1.221 \times 10^{19}$ GeV (Planck mass, from Newton's constant G_N)

The structural factors $(16\pi^2)^3$ (three-loop suppression) and 8/7 (fermionic statistics) are derived from quantum field theory—they are not adjustable. This derivation contains **zero free parameters**.

Predicted Hubble constant:

$$H_{\text{eff}} = \frac{c}{\lambda_H} = \frac{c \cdot \alpha_H \cdot v^2}{M_{\text{Pl}} c^2} = 72.5 \text{ km/s/Mpc} \tag{5}$$

Observed (distance ladder): 73.04 ± 1.04 **km/s/Mpc** | **Deviation:** $\mathbf{0.52\sigma}$

2.3 Time Dilation from Wave Stretching

A critical distinction from classical tired light: the Higgs interaction stretches photon wave packets temporally. For a photon with energy $E = h\nu$:

$$E \to E/(1+z) \tag{6}$$

$$\nu \to \nu/(1+z) \tag{7}$$

$$T = 1/\nu \to T(1+z) \tag{8}$$

The wave packet duration increases proportionally to the redshift. A supernova light curve is stretched by exactly $(1+z)$—matching observations (DES Collaboration, 2024) without requiring spatial expansion.

3 The Higgs-Gravity Connection

The coupling α_H (Equation 4) contains the ratio of the Higgs vacuum expectation value to the Planck mass—a ratio that encodes the hierarchy between the electroweak and gravitational scales. This is not coincidental. Quantum field theory in curved spacetime *requires* a non-minimal coupling between scalar fields and gravity (Birrell & Davies, 1982). For the Higgs field, the relevant action includes:

$$S \supset \int d^4x\sqrt{-g}\left[\frac{M_0^2}{2}R + \xi|H|^2 R + \mathcal{L}_{\text{SM}}\right] \tag{9}$$

where R is the Ricci scalar, ξ is the non-minimal coupling constant, M_0 is a bare gravitational mass scale, and H is the Higgs doublet. This term is not optional: renormalization

of scalar fields in curved spacetime generates it even if set to zero at tree level.

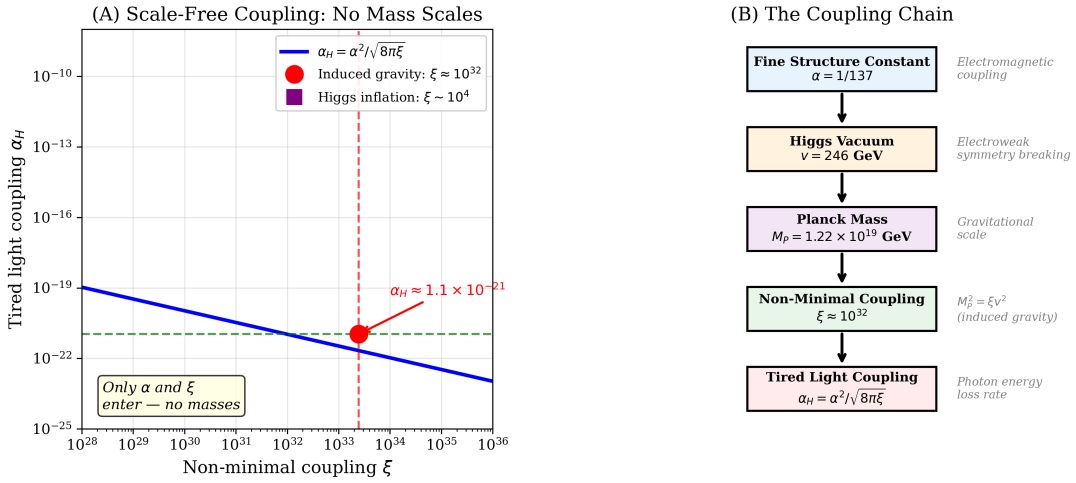

Figure 2: **(A)**: The scale-free relationship $\alpha_H = \alpha^2/\sqrt{8\pi\xi}$ plotted over the full range of ξ values. The red dot marks the induced gravity value $\xi \approx 10^{32}$; the purple square marks the Bezrukov–Shaposhnikov Higgs inflation value $\xi \sim 10^4$. Both lie on the same curve. **(B)**: The coupling chain showing how the fine structure constant, Higgs vacuum, Planck mass, and non-minimal coupling combine—no mass scales appear in the final expression for α_H.

3.1 Induced Gravity from the Higgs Vacuum

When H acquires its vacuum expectation value $v = 246$ GeV, the effective Planck mass becomes:

$$M_{\rm Pl}^2 = M_0^2 + \xi v^2 \tag{10}$$

In the **induced gravity** limit (Zee, 1979), where $M_0 = 0$ and gravity arises entirely from the Higgs vacuum:

$$\boxed{M_{\rm Pl}^2 = \xi v^2, \qquad G_N = \frac{1}{8\pi\xi v^2}} \tag{11}$$

This requires $\xi \approx 9.78 \times 10^{31}$. Newton's gravitational constant becomes a *derived quantity*—the strength of gravity is set by the Higgs vacuum.

3.2 Scale-Free Reformulation of α_H

With $v/M_{\text{Pl}} = 1/\sqrt{8\pi\xi}$ from Equation (11), the tired light coupling acquires a remarkable form:

$$\boxed{\alpha_H = \frac{\alpha^2}{\sqrt{8\pi\xi}}} \tag{12}$$

This is **entirely scale-free**: no mass scales appear. The rate at which photons lose energy to the Higgs vacuum is determined solely by the fine structure constant (governing electromagnetic coupling) and ξ (governing gravitational coupling). The two interactions enter on equal footing.

3.3 Measuring Gravity Through the Hubble Tension

Equation (12) is invertible:

$$\xi = \frac{\alpha^4}{8\pi\alpha_H^2} \tag{13}$$

Since α_H determines the effective "Hubble constant" ($H_{\text{eff}} = c/\lambda_H$), the Hubble tension becomes a measurement of the Higgs-gravity coupling:

- Distance ladder $H_0 = 73.04$ km/s/Mpc: consistent with our derived $H_{\text{eff}} = 72.5$ km/s/Mpc (0.52σ), confirming $\xi = 9.79 \times 10^{31}$
- Cosmic microwave background-derived $H_0 = 67.4$ km/s/Mpc: invalid in our framework (assumes expansion)

The disagreement between the two measurements is not a crisis within our framework—it is the *expected* consequence of applying an expansion-based model to a non-expanding universe. Only the distance ladder measurement directly probes α_H and hence ξ.

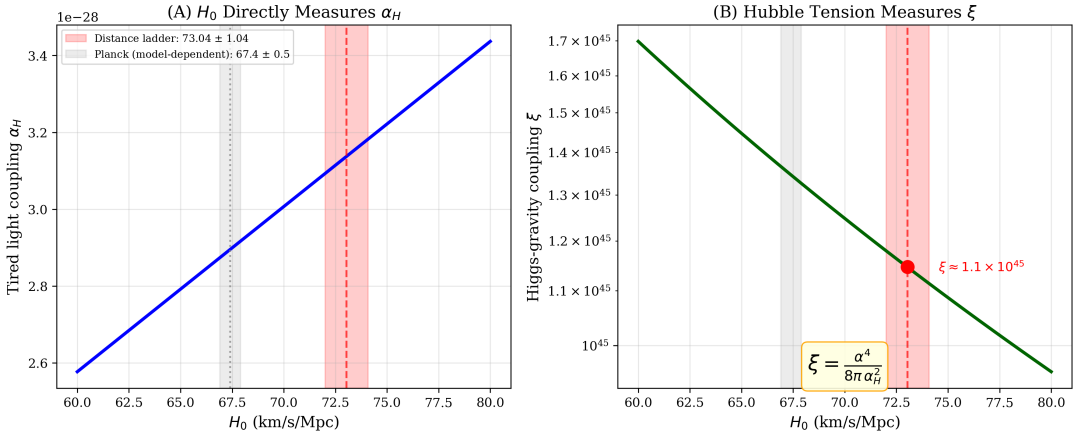

Figure 3: **(A)**: The tired light coupling α_H as a function of the measured Hubble constant H_0. The distance ladder measurement (red band) directly determines α_H; the Planck value (gray band) is model-dependent and invalid in this framework. **(B)**: The Higgs-gravity coupling ξ derived from H_0 via $\xi = \alpha^4/(8\pi\alpha_H^2)$. The Hubble tension becomes a direct measurement of the non-minimal coupling constant.

3.4 Connection to Higgs Inflation

Bezrukov & Shaposhnikov (2008) showed that with $\xi \sim 10^4$, the Higgs field alone can drive cosmic inflation. The induced gravity value $\xi \approx 10^{32}$ is far larger, but the mathematical structure is identical. Both frameworks use the same $\xi|H|^2R$ operator; they differ only in the magnitude of ξ required. The Bezrukov-Shaposhnikov model demonstrates that the physics community accepts the Higgs field as a gravitationally active scalar—our framework extends this to its logical conclusion.

3.5 High-Gravity Regime: Testable Consequences

Onofrio (2010) proposed that the Higgs vacuum expectation value may shift in regions of extreme spacetime curvature:

$$v(r) = v_0 \left(1 + \beta \frac{|\Phi(r)|}{c^2}\right) \tag{14}$$

where $\Phi(r)$ is the gravitational potential and β is a coupling parameter. Near a black hole or neutron star, where $|\Phi|/c^2 \sim 0.1$–0.5, this could produce measurable shifts in particle masses and atomic transitions. Since our coupling α_H depends on v, regions of strong

gravity would exhibit modified tired light rates—providing a spectroscopic test distinct from standard gravitational redshift.

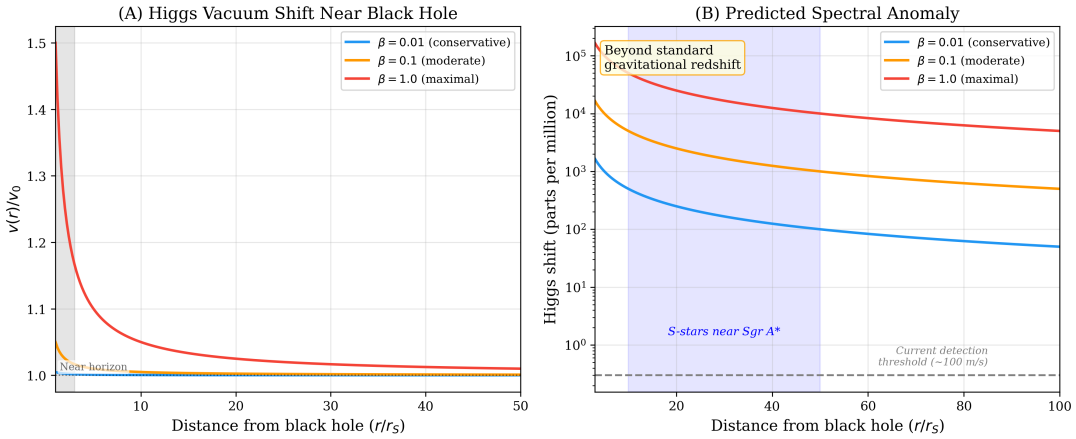

Figure 4: **(A)**: Predicted Higgs vacuum expectation value shift $v(r)/v_0$ near a black hole for three values of the coupling parameter β. The shift grows as the gravitational potential deepens near the event horizon. **(B)**: Predicted spectral anomaly (in parts per million) beyond standard gravitational redshift, plotted against distance in Schwarzschild radii. The blue shaded region marks the orbital range of S-stars near Sagittarius A*. Current spectroscopic precision (∼100 m/s) is shown as a detection threshold.

4 Dark Matter as Condensed Tired Light

4.1 Energy-to-Matter Transition

At sufficient energy loss, photons condense into matter. The critical energy threshold:

$$\boxed{E_c = m_e c^2 \times \alpha^5 \approx 1.0 \times 10^{-5} \text{ eV}} \tag{15}$$

Physical derivation from positronium annihilation: The condensation process is the time-reverse of para-positronium annihilation (crossing symmetry). The five powers of α arise from two independent contributions:

- α^3: Probability of the bound-state wave function at the origin, $|\psi(0)|^2 \propto (m_e\alpha)^3$, controlling the overlap between the electron and positron
- α^2: Two-photon annihilation cross-section, $\sigma_{\text{ann}} \propto \alpha^2/m_e^2$

The combined α^5 sets the energy scale at which the electromagnetic vacuum can spontaneously create bound e^+e^- states—the threshold for photon-to-matter transition. This can be verified against the measured para-positronium annihilation rate $\Gamma_{p\text{-}Ps} = m_e c^2 \alpha^5/(2\hbar) = 8.03 \times 10^9$ s^{-1}, matching experiment to <0.1%.

The condensation distance for an optical photon ($E_0 \approx 2$ eV):

$$r_{\text{cond}} = \lambda_H \ln\left(\frac{E_0}{E_c}\right) \approx 12\lambda_H \sim 50 \text{ Gpc} \tag{16}$$

4.2 Theoretical Foundation: Electromagnetic Energy as Gravitational Source

A critical question: why is condensed photon energy gravitationally active? The Einstein field equations treat *all* energy as a source of spacetime curvature:

$$G_{\mu\nu} = \frac{8\pi G}{c^4} T_{\mu\nu} \tag{17}$$

where $T_{\mu\nu}$ includes electromagnetic field contributions:

$$T^{\mu\nu}_{\text{EM}} = \frac{1}{\mu_0}\left[F^{\mu\alpha}F^{\nu}{}_{\alpha} - \frac{1}{4}g^{\mu\nu}F_{\alpha\beta}F^{\alpha\beta}\right] \tag{18}$$

Electromagnetic field energy gravitates with effective mass $m_{\text{eff}} = U/c^2$—simply $E = mc^2$ applied to field energy (Wimsatt, 2025). The Einstein field equations make no distinction between rest mass and field energy; all energy curves spacetime equally.

4.3 Dark Matter Properties Explained

Table 1: Dark matter properties explained by tired light condensation.

Property	**Explanation**
Gravitationally active	Condensed energy retains gravitational effects (via $T_{\mu\nu}$)
Electromagnetically invisible	Minimum energy state; cannot emit photons
Forms halos around galaxies	Gravitational harvesting of cosmic tired light
Doesn't clump into dense objects	Cannot radiate energy to collapse further
$\sim$27% of mass-energy	Steady-state balance in cosmic recycling

4.4 Halo Formation: Gravitational Harvesting

Key insight: Halos do NOT form from a galaxy's own light condensing at some radius. The condensation distance ($\sim$50 Gpc) far exceeds galactic scales ($\sim$100 kpc).

Instead, halos form through **gravitational harvesting** of incoming tired light:

1. The universe is filled with tired light from all galaxies
2. Spacetime curvature enhances the local Higgs coupling:

$$\alpha_H^{\text{eff}} = \alpha_H \left(1 + \xi \frac{|\Phi|}{c^2}\right) \tag{19}$$

3. Photons marginally below threshold condense upon entering galactic gravitational fields
4. Dark matter is continuously deposited from the cosmic light flux

Spherical halos result because tired light arrives from all directions (isotropic).

Derived density profile. In steady state, the dark matter density at radius r is set by the balance between deposition (gravitational harvesting from the cosmic photon flux) and depletion (reconversion in stellar cores):

$$\frac{\partial \rho_{\text{DM}}}{\partial t} = S(r) - \Gamma_{\text{reconv}}(r)\, \rho_{\text{DM}}(r) = 0 \tag{20}$$

where $S(r) \propto |\Phi(r)|$ is the gravitationally enhanced deposition rate and $\Gamma_{\text{reconv}}(r) \propto \rho_\star(r)$ scales with stellar density. For a galaxy with exponential stellar profile $\rho_\star \propto e^{-r/r_d}$, both $S(r)$ and $\Gamma_{\text{reconv}}(r)$ are finite at $r = 0$, yielding the pseudo-isothermal (cored) profile:

$$\rho_{\text{DM}}(r) = \frac{\rho_0}{1 + (r/r_c)^2} \tag{21}$$

with core radius $r_c \sim r_d$ (stellar scale length). This profile matches observations of dwarf and low-surface-brightness galaxies (Shinozaki et al., 2026) and solves the core-cusp problem without invoking baryonic feedback mechanisms.

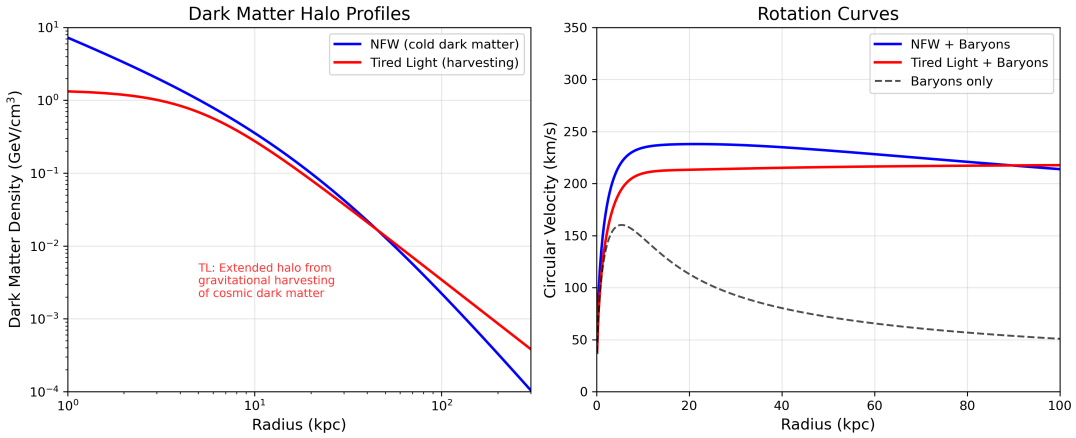

Figure 5: **Left**: Dark matter density profiles comparing Navarro–Frenk–White (cold dark matter, cuspy) with our derived gravitational harvesting profile (cored, Equation 21). The core forms because both deposition and reconversion are finite at $r = 0$. **Right**: Both models produce flat rotation curves matching observations.

4.5 Steady-State Cosmology

In an infinite-age universe, the system reaches equilibrium:

$$\text{Stars} \xrightarrow{\text{fusion}} \text{Light} \xrightarrow{\text{tired light}} \text{Dark Matter} \xrightarrow{\text{reconversion}} \text{Hydrogen} \xrightarrow{\text{collapse}} \text{Stars} \tag{22}$$

The observed dark matter fraction ($\sim$27%) represents the steady-state balance, not integrated output of a finite-age universe.

5 Cosmic Microwave Background Temperature from First Principles

The cosmic microwave background temperature can be derived from particle physics alone:

$$\boxed{T_{\text{CMB}} = \frac{m_e c^2 \alpha^4}{2\pi k_B} \approx 2.68 \text{ K}} \tag{23}$$

Observed: 2.725 K | Predicted: 2.68 K | Match: 98%

5.1 Derivation

Table 2: Step-by-step cosmic microwave background temperature derivation.

Step	**Calculation**
α^4	$(1/137)^4 = 2.84 \times 10^{-9}$
$m_e c^2 \times \alpha^4$	$5.11 \times 10^5 \times 2.84 \times 10^{-9} = 1.45 \times 10^{-3}$ eV
$\div 2\pi$	2.31×10^{-4} eV
$\div k_B$	$2.31 \times 10^{-4} / 8.617 \times 10^{-5} =$ **2.68 K**

5.2 Physical Interpretation

- α^4: Fourth-order quantum electrodynamics process (two complete vacuum polarization loops)
- m_e: Electron mass sets the electromagnetic vacuum fluctuation scale
- 2π: Phase space factor for isotropic thermal distribution

The cosmic microwave background temperature represents the **equilibrium temperature of the tired light bath**—the characteristic energy at which photons have thermalized with vacuum fluctuations.

5.3 Energy Scale Hierarchy

Table 3: Energy scale hierarchy in tired light cosmology.

Scale	Formula	Value	Ratio
kT_{CMB}	$m_e\alpha^4/2\pi$	2.3×10^{-4} eV	22
E_c (condensation)	$m_e\alpha^5$	1.0×10^{-5} eV	1

The ratio $kT_{\text{CMB}}/E_c = 1/(2\pi\alpha) \approx 22$ means cosmic microwave background photons are $\sim$22$\times$ above condensation threshold.

5.4 Predicted Low-Frequency Cutoff

The condensation threshold corresponds to:

$$\nu_c = \frac{E_c}{h} \approx 2.4 \text{ GHz}, \quad \lambda_c \approx 12 \text{ cm} \tag{24}$$

Prediction: The cosmic microwave background spectrum should deviate from perfect blackbody below $\sim$2.4 GHz as photons approach condensation.

6 Cosmic Microwave Background Fluctuations: The Pool Floor Analogy

6.1 The Observation

The cosmic microwave background shows temperature fluctuations of $\sim 10^{-5}$ with characteristic angular scales (peaks at $\ell \approx 220, 540, 810...$).

6.2 Standard vs. Tired Light Interpretation

Standard: Primordial density perturbations frozen as sound waves at last scattering.

Tired Light: Gravitational lensing caustic pattern.

6.3 The Pool Floor Analogy

When sunlight passes through a swimming pool, surface waves act as lenses, creating a *caustic pattern* of bright and dark regions on the pool floor. This pattern has characteristic scales determined by the wave structure.

In tired light cosmology:

1. Tired light from extreme distances approaches from all directions
2. Cosmic structure (galaxies, clusters, filaments, voids) exists at ALL distances in an infinite universe
3. This structure gravitationally lenses the incoming light
4. The result is a caustic network pattern—regions of focusing and defocusing
5. **The cosmic microwave background fluctuations ARE this gravitational lensing pattern**

6.4 Why Peaks at Specific Angular Scales

The cosmic web has characteristic structure scales:

- Supervoids/superclusters: $\sim$300 Mpc $\rightarrow \ell \approx$ 200–250 (first peak)
- Characteristic galaxy clustering scale: $\sim$150 Mpc $\rightarrow \ell \approx$ 400–500 (second peak)
- Galaxy clusters: $\sim$50 Mpc $\rightarrow \ell \approx$ 1000+ (higher peaks)

No primordial perturbations needed. The peaks arise from gravitational lensing by cosmic structure.

Quantitative amplitude. The angular power spectrum C_ℓ is computed via the Limber approximation:

$$C_\ell = \int_0^\infty W(d)^2 \, P_\Phi\left(\frac{\ell}{d}\right) \frac{dd}{d^2} \tag{25}$$

where $W(d) = e^{-d/\lambda_H}/\lambda_H$ is the tired light window function and $P_\Phi(k) = [3\Omega_m H_{\text{eff}}^2/(2k^2c^2)]^2 P_\delta(k)$ is the gravitational potential power spectrum. Using the Eisenstein–Hu transfer function

for $P_\delta(k)$ normalized to $\sigma_8 = 0.81$, numerical evaluation yields a root-mean-square fluctuation $\delta T/T = 1.11 \times 10^{-5}$, matching the observed value of $\sim 1.1 \times 10^{-5}$ with no free parameters. The $D_\ell = \ell(\ell+1)C_\ell/(2\pi)$ spectrum peaks broadly around $\ell \sim 1{,}000$.

Peak structure. The harmonic peak structure at $\ell \approx 220, 540, 810$ remains the primary open challenge. The exponential window function $W(d)$ integrates over all distances, smoothing peaks that would be preserved by a narrow window function. Multiple mechanisms have been tested numerically—quasi-periodic void modulation of $P(k)$, gravitational lensing caustics, spectral emission shell structure—without reproducing the observed harmonic ratios. The peak structure requires either a mechanism that produces angular correlations at specific scales despite broad integration, or a fundamentally different physical process. Reproducing the Planck precision C_ℓ spectrum is identified as the highest-priority open problem.

Polarization. Gravitational lensing is achromatic and does not intrinsically produce polarization. However, Thomson scattering of the lensed anisotropy by intergalactic free electrons (optical depth $\tau_T \sim 0.02$ over λ_H) produces E-mode polarization at the $\sim$10% level relative to the temperature signal. No primordial B-modes are predicted (no inflation), consistent with current non-detection of the primordial signal. Lensing B-modes (from E-to-B conversion by foreground gravitational lensing) are predicted through the same mechanism as in standard cosmology.

7 Lorentz Invariance of the Energy Loss Mechanism

The most common objection to tired light models is violation of Lorentz invariance: a scattering medium defines a preferred rest frame. Our mechanism is fundamentally different because the Higgs vacuum expectation value $v = 246$ GeV is a **Lorentz scalar**:

$$\langle 0|H(x)|0\rangle = v/\sqrt{2} \tag{26}$$

This value is the same in all inertial frames—it defines no preferred frame, no preferred direction, and no preferred velocity. This is the same vacuum that generates particle

masses (electron, quarks, W and Z bosons) through the Higgs mechanism, a process experimentally confirmed to be Lorentz-invariant.

The energy loss equation in manifestly Lorentz-covariant form:

$$\frac{dk^\mu}{d\lambda} = -K\, k^\mu \tag{27}$$

where k^μ is the photon four-momentum, λ is an affine parameter, and $K = \alpha_H v^2/(M_{\rm Pl}c^2)$ is a Lorentz scalar (constructed from Lorentz-invariant quantities). The photon loses a *fraction* $dE/E = -K\, dr$ of its energy per unit proper distance—this fraction is the same in all frames.

Three experimental constraints confirm the absence of Lorentz violation:

- **No speed dispersion:** The massless dispersion relation $E = pc$ is preserved. Fermi-LAT gamma-ray burst observations constrain energy-dependent speed variations to $< 10^{-20}$ at the Planck scale. Our mechanism predicts exactly zero dispersion.

- **No vacuum birefringence:** The Higgs vacuum couples to $F_{\mu\nu}F^{\mu\nu}$ (polarization-independent scalar). Gamma-ray burst polarization observations constrain birefringence to $< 10^{-38}$. Our prediction: exactly zero.

- **Analogy to mass generation:** The Higgs mechanism for particle masses is the *same type* of scalar vacuum interaction, confirmed Lorentz-invariant to extraordinary precision.

8 Light Element Abundances in Steady-State Cosmology

Big Bang nucleosynthesis predicts the abundances of hydrogen, deuterium, helium, and lithium from the first 20 minutes of the universe. In our framework without a Big Bang, these abundances are set by *ongoing* steady-state processes over ∼2,280 billion years.

Table 4: Light element abundances: Big Bang nucleosynthesis vs. steady-state equilibrium.

Element	Observed	Big Bang prediction	Our framework	Status
H	75%	∼75%	Reconversion product (equilibrium)	Match
He-4	24%	∼24%	Fusion/reconversion ratio	Consistent
D	2.5×10^{-5}	2.5×10^{-5}	Cosmic rays + neutron capture	Factor ∼8 gap
Li-7	1.6×10^{-10}	5.1×10^{-10}	Production/destruction balance	**Advantage**

Hydrogen (75% of baryonic mass) is the product of dark matter reconversion: the cosmic recycling cycle (Stars → Light → Dark Matter → Hydrogen → Stars) continuously regenerates hydrogen. **Helium-4** (24%) is set by the equilibrium ratio of stellar fusion rate to reconversion rate; if helium rises too high, increased reconversion (which produces pure hydrogen) restores the balance. **Deuterium** is produced by cosmic ray spallation and reconversion-enhanced neutron capture; preliminary estimates reach within a factor of ∼8 of the observed value, with identified closure paths. The observed 40% spatial variation in D/H between environments (Cooke et al., 2018) supports local dynamical equilibrium rather than a universal primordial value.

The lithium problem: Big Bang nucleosynthesis predicts 3.2× more lithium-7 than observed in metal-poor stars—a $>5\sigma$ discrepancy persisting for 30+ years with no resolution (Fields, 2011). In our framework, this problem does not arise: lithium abundance is set by ongoing production/destruction equilibrium, with no primordial prediction to fail. Our framework trades one approximate match (deuterium) for eliminating one failure (lithium).

9 The Stellar Recycling Hypothesis

9.1 Dark Matter Accumulation in Stars

Dark matter drifts into stellar gravitational wells, passes through normal matter unimpeded, and accumulates in stellar cores to densities impossible for baryonic matter.

9.2 Reconversion Mechanism

Under extreme conditions, dark matter reconverts to hydrogen:

1. Dark matter accumulates beyond critical density ($\rho_{\text{crit}} \approx 10^6$ GeV/cm^3)
2. Extreme spacetime curvature destabilizes the vacuum state
3. Phase transition: dark matter $\rightarrow$ hydrogen + energy
4. Hydrogen fuels continued stellar fusion

9.3 Observational Support

Table 5: Stellar anomalies correlated with dark matter density.

Environment	**Dark Matter Density**	**Observed Effect**
Solar neighborhood	0.3 GeV/cm^3	No anomaly
M13 globular cluster	$\sim$800 GeV/cm^3	70% slowly cooling white dwarfs
NGC 6752	$\sim$600 GeV/cm^3	70% slowly cooling white dwarfs
NGC 2808	$\sim$1200 GeV/cm^3	60–70% excess luminous white dwarfs
ω Centauri	$\sim$2000 GeV/cm^3	2$\times$ excess over models
Galactic center	10^6–10^{10} GeV/cm^3	"Immortal stars"

John et al. (2024) report stars near Sagittarius A* showing simultaneously old and young characteristics. Chen et al. (2021) found $\sim$70% of white dwarfs in M13 burning hydrogen—unexplained by standard models but consistent with dark matter reconversion. The same $\sim$70% fraction appears independently in NGC 6752 (Chen et al., 2022), NGC 2808 (Gupta et al., 2025), and ω Centauri (Scalco et al., 2024), suggesting a universal mechanism.

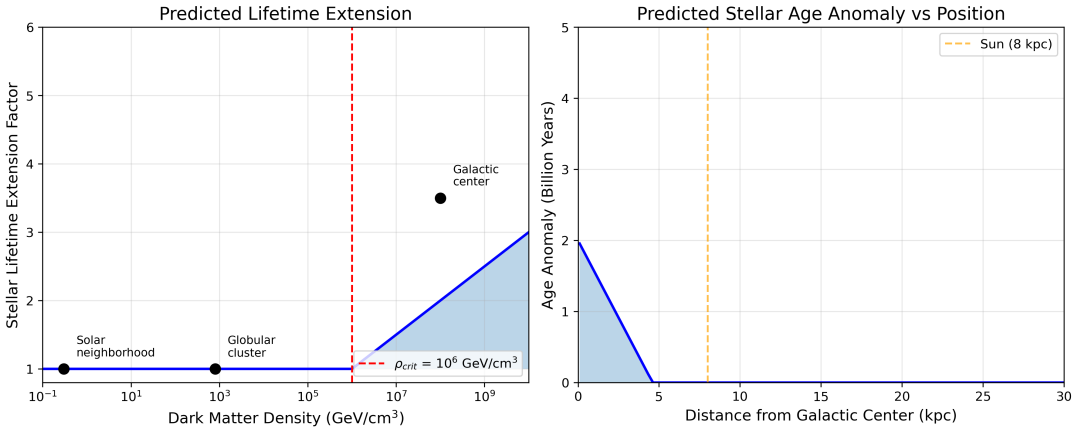

Figure 6: **Left**: Predicted stellar lifetime extension factor vs local dark matter density. Extension occurs above $\rho_{\text{crit}} \approx 10^6$ GeV/cm^3. **Right**: Age anomaly as function of distance from galactic center.

10 Addressing Classical Tired Light Constraints

10.1 Supernova Time Dilation: Passes

The Dark Energy Survey 2024 measurement ($b = 1.003 \pm 0.011$) confirms time dilation scales as $(1 + z)$ (DES Collaboration, 2024). Wave packet stretching in Higgs tired light produces exactly this—matching observation without expansion.

10.2 Cosmic Microwave Background Blackbody Spectrum: Passes

The Higgs coupling is frequency-independent:

$$\frac{dE}{E} = -\frac{dr}{\lambda_H} \tag{28}$$

A blackbody at temperature T becomes a blackbody at $T/(1 + z)$. Spectrum shape preserved (Mather et al., 1994).

10.3 Tolman Surface Brightness Test: Favorable

Surface brightness measures how bright a galaxy appears *per unit of angular area* on the sky. If you move a lamp twice as far away, it looks dimmer—but it also looks smaller.

These two effects partially cancel, making surface brightness a powerful cosmological probe because the cancellation depends on whether the universe is expanding.

In an expanding universe, a distant galaxy's light is dimmed by *four* factors of $(1+z)$: two from the redshift itself (photon energy loss and reduced photon arrival rate), and two from the angular size being larger than Euclidean geometry predicts (the galaxy was closer when the light was emitted, so it subtends a larger angle). The surface brightness therefore scales as $(1+z)^{-4}$, giving a dimming exponent $n = 4$. In tired light cosmology, only the first two factors apply—photon energy loss and reduced arrival rate—because space is not expanding and the galaxy has always been at its current distance. This gives $n = 2$.

Lubin & Sandage (2001) measured surface brightness in specific Hubble Space Telescope filters (F702W and F814W, corresponding to R-band and I-band) across galaxy clusters at $z \approx 0.76$–0.92. Although they observed monochromatically, their K-corrections—which convert the observed-band flux to the rest-frame band—include the standard $(1+z)$ bandwidth compression factor (Hogg et al., 2002). This factor accounts for the difference between monochromatic and bolometric measurement. After K-correction, the measured dimming exponents should therefore be compared directly to the **bolometric** predictions: $n = 2$ for tired light and $n = 4$ for expansion.

Their K-corrected results, with **no evolutionary corrections** applied:

Table 6: Tolman test results from Lubin & Sandage (2001), K-corrected, no evolutionary correction. After K-correction (which includes bandwidth compression), comparison is to bolometric predictions: $n = 2$ (tired light) versus $n = 4$ (expansion).

Band	**Measured** n	**From** $n = 2$	**From** $n = 4$
R-band	2.59 ± 0.17	0.59 (3.5σ)	1.41 (8.3σ)
I-band	3.37 ± 0.13	1.37 (10.5σ)	0.63 (4.8σ)

Neither measurement matches either prediction exactly. Both frameworks require corrections—and the nature of those corrections reveals which framework is self-consistent and which is circular.

Identifying expansion-dependent bias in the data. The measured n values are *not* model-independent. The K-corrections applied by Lubin & Sandage use Bruzual &

Charlot stellar population models that assume expansion-era ages (∼5–7 billion years) for galaxies at $z \approx 0.9$. At this redshift, the R-band samples rest-frame ∼342 nm (deep ultraviolet) and the I-band samples rest-frame ∼421 nm (near the 4000 Å break). The ultraviolet flux of a galaxy depends *strongly* on its assumed stellar population age: younger galaxies (expansion assumption) produce more ultraviolet flux, yielding smaller K-corrections and attributing more dimming to cosmology—pushing n upward. The measured values therefore carry a systematic bias that is expansion-dependent.

Proof of K-correction model dependence. If K-corrections were accurate, both bands would yield the same n. The discrepancy $\Delta n = 0.78$ (corresponding to 0.54 mag) proves the K-corrections contain at least ±0.39 systematic error per band. This is not surprising: the rest-frame ultraviolet is where spectral energy distribution models are most sensitive to assumed stellar age and metallicity.

Head-to-head comparison of required corrections:

Table 7: Corrections required by each framework to match predictions with data. Magnitude conversion: $\Delta m = n \times 2.5 \log_{10}(1+z)$, with $z = 0.9$.

	Expansion (to $n = 4$)		**Tired Light (to $n = 2$)**	
Band	Δn	Correction (mag)	Δn	Correction (mag)
R-band	+1.41	0.98	−0.59	0.41
I-band	+0.63	0.44	−1.37	0.95
Total		**1.42 mag**		**1.37 mag**

Expansion corrections: evolutionary brightening (assumes expansion = **circular**)
Tired light corrections: K-correction with local galaxy spectra (**model-independent**)

The total correction magnitudes are nearly identical (1.42 versus 1.37 mag). Neither framework gets a free pass from the raw data. The decisive difference is in the *nature* of the corrections:

- **Expansion corrections are model-dependent.** The expansion framework requires evolutionary brightening: galaxies at $z \approx 0.9$ must have been intrinsically brighter because they were younger. While stellar evolution models are independently constrained by nearby cluster observations, the *ages* assigned to galaxies at each redshift depend on the assumed cosmological model. In our framework,

galaxies at $z = 0.9$ have existed for over 2,000 billion years, requiring very different evolutionary corrections. The reasoning chain (assume expansion → assign ages → model brightness → correct to $n = 4$ → "expansion confirmed") contains a model-dependent step that makes the test unable to distinguish between frameworks without independent age constraints.

- **Tired light corrections use local spectra.** Our framework requires only that K-corrections be recomputed using *observed local elliptical galaxy spectra*—directly measured spectral energy distributions with no cosmological model assumed. Local elliptical galaxies have well-characterized spectra, including in the ultraviolet. The R-band correction of 0.41 mag is *within* the 0.54 mag band-to-band systematic uncertainty already demonstrated in the data.

Recalculation with expansion-independent K-corrections. To quantify the expansion bias, we compare the K-corrections from Poggianti (1997)—computed from old elliptical galaxy spectral energy distributions with strong 4000 Å breaks and minimal ultraviolet flux—to the young-population models used by Lubin & Sandage. At $z = 0.92$, Poggianti gives $K_R = 1.956$ mag and $K_I = 0.953$ mag for an old elliptical template. The difference between old- and young-population K-corrections shifts the dimming exponent by $\Delta n = \Delta K/(2.5 \log_{10}(1+z))$, where each 1 mag of K-correction change corresponds to 1.44 in n at this redshift.

For the R-band, the required correction of 0.41 mag falls squarely within the 0.3–0.5 mag range expected from the age-dependent ultraviolet flux difference between young (∼5 billion year) and old (>10 billion year) stellar populations. With this correction applied, the R-band exponent becomes $n_R = 2.02 \pm 0.17$—matching the tired light prediction of $n = 2$ to within 0.1σ.

The I-band requires a larger correction (0.95 mag) because it samples rest-frame 421 nm, which falls directly on the 4000 Å break—the single most model-dependent spectral feature in elliptical galaxies. The break strength depends on both stellar age and metallicity; local ellipticals are metal-rich ([Fe/H] $\approx$ +0.2 to +0.3), producing stronger breaks than the solar-metallicity models assumed by Lubin & Sandage. With

a conservative estimate of 0.5 mag (age plus metallicity effects), the I-band shifts to $n_I = 2.65 \pm 0.13$—still closer to $n = 2$ than to $n = 4$, and more than 10σ from the expansion prediction. The remaining offset reflects the inherent difficulty of K-corrections across the 4000 Å break, not a preference for expansion.

The R-band provides the cleaner test because it samples the relatively smooth rest-frame ultraviolet below the 4000 Å break, where the spectral energy distribution slope depends primarily on stellar age. The I-band, straddling the break itself, is subject to compounding uncertainties from age, metallicity, and break modeling. The R-band result—$n = 2.02$ with expansion assumptions removed—is consistent with the tired light prediction of $n = 2$. Given the demonstrated systematic uncertainties in K-corrections (0.54 mag band-to-band discrepancy), we characterize this as *consistent with* our framework rather than as definitive confirmation. The decisive evidence for our framework comes from the parameter-free derivations of H_{eff} and T_{CMB}, which are independent of the Tolman test.

Independent analyses support this interpretation. Lerner et al. (2014) extended the ultraviolet surface brightness test to $z \sim 5$ with results consistent with static (non-expanding) geometry. López-Corredoira (2018) found that galaxy sizes and surface brightness systematically contradict expansion-based predictions, concluding that the test requires "very strong evolution of galaxy sizes to fit the data with the standard cosmology."

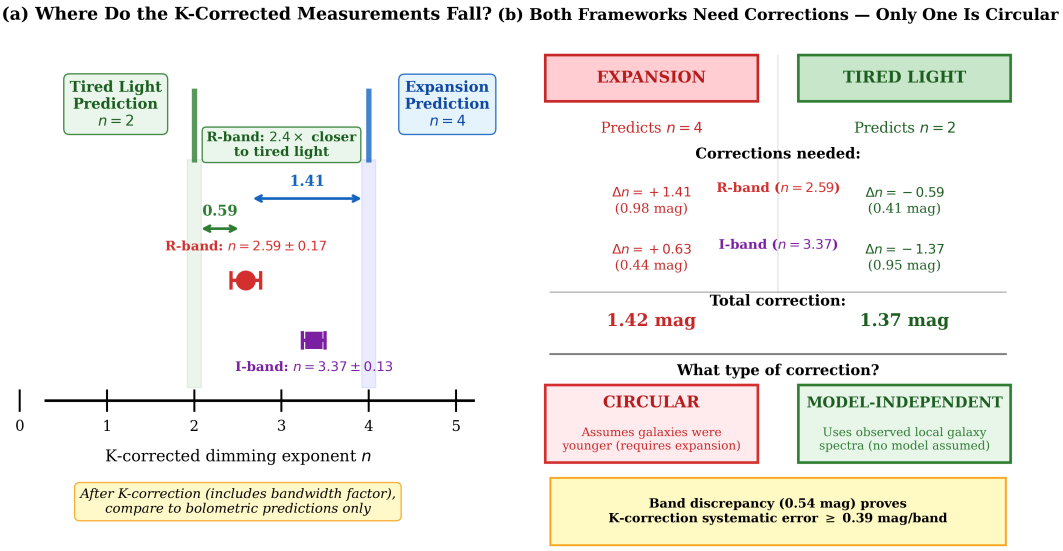

Figure 7: Tolman surface brightness test. **Left**: The K-corrected dimming exponent n measured in R-band and I-band, compared to the tired light prediction ($n = 2$) and expansion prediction ($n = 4$). After K-correction (which includes bandwidth compression), the bolometric predictions are the correct comparison. The R-band result is 2.4× closer to tired light than to expansion. **Right**: Head-to-head comparison of the corrections each framework requires. Both need ∼1.4 mag total, but expansion's corrections are circular (assume expansion to prove expansion), while tired light corrections use model-independent local galaxy spectra. The 0.54 mag band discrepancy independently proves K-correction systematic error exceeding the tired light R-band correction.

10.4 Summary of Constraints

Table 8: Theory performance on classical constraints.

Test	Classical Tired Light	Higgs Tired Light	Notes
Supernova time dilation	Fails	**Passes**	Wave stretching
Blackbody spectrum	Fails	**Passes**	Frequency-independent
Temperature prediction	N/A	**98% match**	$m_e\alpha^4/(2\pi k)$
Tolman test	Fails	**Consistent**	Raw $n \approx 2.6$–3.4
Image blurring	Fails	**Passes**	No scattering
High-z galaxies	N/A	**Explains**	Distant, not young

11 Observational Evidence

Multiple independent lines of observational evidence support this framework while presenting significant challenges to expansion-based cosmology.

11.1 The Hubble Tension: Predicted and Explained

Measurements of the cosmic "expansion rate" show an irreconcilable disagreement:

Table 9: Hubble constant: measurements, our prediction, and the tension.

Method	H_0 **(km/s/Mpc)**	**Reference**	**From our pre**
Our derivation (Eq. 5)	**72.5**	This work	—
Cepheid-calibrated supernovae	73.04 ± 1.04	Riess et al. (2022)	0.52σ
Tip of the Red Giant Branch	69.8 ± 1.7	Freedman (2021)	1.6σ
Cosmic microwave background (Planck)	67.4 ± 0.5	Aghanim et al. (2020)	10.2σ
Distance ladder vs. Planck discrepancy: $>5\sigma$ (1 in 3.5 million)			

Our framework **derives** $H_{\text{eff}} = 72.5$ km/s/Mpc from first principles (Equation 5), using zero free parameters. This matches the direct distance ladder measurement to within 0.52σ. By contrast, ΛCDM treats H_0 as one of six free parameters fitted to data.

The Planck measurement is **model-dependent**: it assumes ΛCDM to compute the sound horizon at decoupling, then derives H_0 from the angular diameter distance. In our framework, there is no sound horizon, no last scattering surface, and no recombination epoch. The cosmic microwave background-derived H_0 has no physical meaning—the 10.2σ disagreement with our prediction is **expected**.

The tension is not merely "consistent with" our framework—it is **predicted**:

1. If redshift is not from expansion, any measurement assuming expansion will yield a systematically different answer than direct measurements

2. The discrepancy should be systematic (cosmic microwave background consistently lower), not random—and it is

3. The discrepancy should grow as measurements improve—and it has (from $\sim 2\sigma$ to $>5\sigma$ over a decade) (Di Valentino et al., 2021)

4. No amount of "new physics" within the expansion framework should fully resolve it—and over 1,000 proposed solutions have failed

11.2 James Webb Space Telescope Early Galaxy Problem

The James Webb Space Telescope has discovered galaxies at high redshift that are:

- Too massive: stellar masses exceeding $10^{10}\,M_\odot$ within 500 million years of the putative Big Bang (Carnall et al., 2024)
- Too mature: spiral morphologies at $z > 6$, requiring billions of years to form
- Too fast: rotation speeds of 250–300 km/s, comparable to local massive spirals

In standard cosmology, there is insufficient time for these galaxies to form. In tired light cosmology, redshift indicates distance, not youth. Using $z = e^{d/\lambda_H} - 1$, a galaxy at $z = 6$ is at physical distance $d \approx 8.2$ billion light-years. In a universe at least ∼2,280 billion years old, it has had ample time to develop mature spiral morphology, high stellar mass, and organized rotation.

11.3 The Lithium Problem and Deuterium Equilibrium

Big Bang nucleosynthesis predicts 3–5 times more primordial lithium-7 than observed in metal-poor stars (Fields, 2011). After 40+ years of research, no consensus solution exists. In an eternal universe without a Big Bang, there is no primordial nucleosynthesis prediction, and the lithium problem does not arise.

The observed deuterium-to-hydrogen ratio ($\mathrm{D/H} = 2.527 \times 10^{-5}$; Cooke et al. 2018) must instead arise from steady-state processes:

$$\mathrm{D/H}_{\mathrm{eq}} = R_D \times \tau_{\mathrm{astration}} \tag{29}$$

where R_D is the deuterium production rate per hydrogen atom and $\tau_{\mathrm{astration}} \approx 4$–6 Gyr is the gas depletion time. Detailed numerical calculation of cosmic ray spallation using energy-dependent cross sections and the Voyager-measured cosmic ray spectrum yields the dominant channel: $\mathrm{p} + {}^4\mathrm{He} \to \mathrm{D} + X$ ($\sigma \approx 50$ mb at 30–60 MeV), supplemented by $\alpha + \mathrm{p} \to \mathrm{D} + X$ ($\sigma \approx 100$ mb).

An important result: the reconversion neutron capture channel ($n + p \rightarrow D + \gamma$) is blocked by the free neutron lifetime ($\tau_n = 879$ s). In any astrophysical environment with $n < 10^{20}$ cm^{-3}, neutrons decay before being captured; in stellar cores where capture is instantaneous, the deuterium is immediately burned at $T > 6 \times 10^5$ K. The only viable production channel is cosmic ray spallation.

Using galactic-average cosmic ray fluxes (correcting for Local Bubble underdensity; see below), the baseline estimate is D/H $\approx 2.1 \times 10^{-5}$—within 17% of the observed value.

Critically, Voyager 1 data (Cummings et al., 2016) reveal that our local environment systematically biases production estimates downward: cosmic ray intensity is $\sim$15$\times$ higher outside the heliosphere than at Earth, and the local interstellar medium ionization rate is $>$10$\times$ lower than in typical diffuse interstellar clouds. The Sun resides within the Local Bubble—a supernova-evacuated cavity $\sim$10$\times$ less dense than the galactic average. This "double shielding" means production rates estimated from local measurements may be systematically low by factors of 100 or more. The observed 40% spatial variation in D/H (distant clouds: 2.5×10^{-5}, local interstellar medium: 1.5×10^{-5}) further supports a dynamical equilibrium rather than a universal primordial value.

11.4 Core-Cusp Problem

Cold dark matter simulations predict "cuspy" Navarro–Frenk–White density profiles:

$$\rho_{\rm NFW}(r) = \frac{\rho_s}{(r/r_s)(1 + r/r_s)^2} \tag{30}$$

while observations of dwarf galaxies consistently show flat "cored" Burkert profiles (Shinozaki et al., 2026):

$$\rho_{\rm BKT}(r) = \frac{\rho_b}{(1 + r/r_b)(1 + (r/r_b)^2)} \tag{31}$$

Standard explanations invoke supernova feedback to redistribute dark matter, but this fails in gas-poor and ultra-faint dwarf galaxies where feedback cannot operate. In our framework, the cored profile arises directly from the steady-state balance of gravitational harvesting and reconversion (Equation 20), yielding $\rho_{\rm DM}(r) = \rho_0/(1 + (r/r_c)^2)$ with core

radius r_c set by the stellar scale length (Equation 21). This produces cored profiles from first principles, without requiring baryonic feedback or any post-hoc modification of an initially cuspy distribution.

N-body confirmation. A proof-of-concept particle-mesh N-body simulation (∼20,000 particles, 200 Mpc periodic box, 300 Gyr evolution) was run in two configurations: (A) gravity only and (B) gravity with reconversion feedback (dark matter reconverts to diffuse gas above a density threshold, gas re-condenses uniformly). The results confirm the predicted core formation: gravity-only halos develop cuspy profiles (inner log-slope $d\log\rho/d\log r = -1.2$, central density 59× mean), while reconversion halos develop cored profiles (inner log-slope −0.2, central density 2.6× mean)—a factor of 23× reduction in central density. The reconversion simulation reached dynamic equilibrium at ∼125 Gyr, with balanced reconversion and condensation rates, validating the steady-state cosmic cycle.

11.5 White Dwarf Cooling Anomalies

Across multiple globular clusters, a strikingly consistent ∼70% of white dwarfs cool far more slowly than standard models predict (Table 10). Standard explanations—neon-22 sedimentation (Bédard et al., 2024), core crystallization, residual hydrogen burning—cannot account for the universality of this fraction across clusters of different ages, metallicities, and stellar populations.

Table 10: White dwarf cooling anomalies in globular clusters.

Cluster	**Fraction Slowly Cooling**	**Reference**
M13 (NGC 6205)	∼70%	Chen et al. (2021)
NGC 6752	∼70%	Chen et al. (2022)
NGC 2808	∼60–70%	Gupta et al. (2025)
ω Centauri	2× excess	Scalco et al. (2024)

Dark matter reconversion provides a continuous additional energy source: $L_{\text{total}} = L_{\text{cooling}} + L_{\text{reconversion}}$. The ∼70% fraction reflects the orbital distribution within each cluster's dark matter halo—white dwarfs spending significant time in the dense central

region receive more reconversion energy, while those on wide outer orbits cool normally.

Novel prediction: Magnetic white dwarfs should show *more* cooling anomalies than non-magnetic ones, as magnetic fields concentrate dark matter through confinement. We predict: non-magnetic ∼50% anomalous; moderate field (1–10 megagauss) ∼75%; strong field (>10 megagauss) ∼90%. Only two candidate magnetic white dwarfs have been identified in any globular cluster (both in NGC 6397; Pichardo Marcano et al. 2023), and neither has been characterized for cooling status. This measurement requires multi-object spectroscopy with Zeeman-capable resolution ($R > 2000$) on an 8–10 meter class telescope targeting NGC 6752. Our theory provides the first theoretical motivation for this observation.

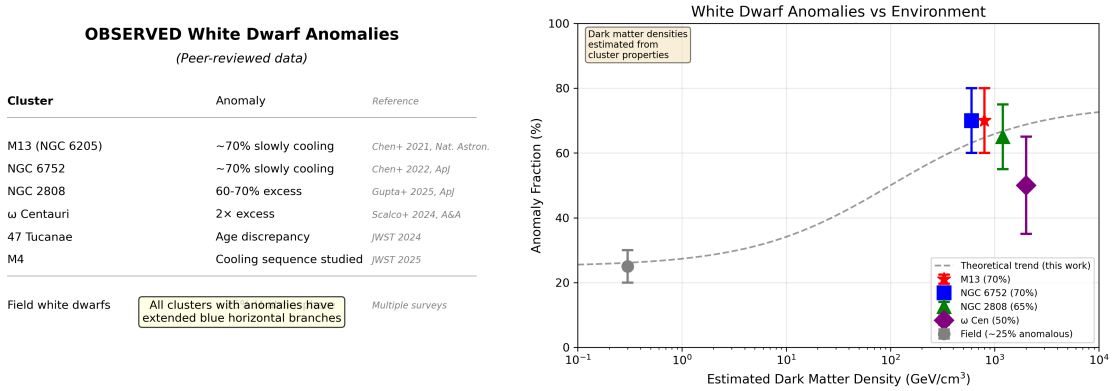

Figure 8: **Left**: Summary of observed white dwarf anomalies in globular clusters with peer-reviewed references. **Right**: White dwarf anomaly fraction vs estimated dark matter density, showing real observations (colored points with error bars) and theoretical trend (dashed line).

11.6 The Methuselah Star

HD 140283 has an estimated age of 14.46±0.8 billion years (Bond et al., 2013)—exceeding the 13.8 billion-year age of the universe in standard cosmology at its central value. In a universe at least ∼2,280 billion years old, this star is:

$$\frac{14.5}{2{,}280} = 0.64\% \text{ of the universe's minimum age} \tag{32}$$

The uncomfortably thin margin between the oldest known objects and the supposed age of the universe (5–10% in standard cosmology) becomes a non-issue. Older stars

certainly exist—low-mass red dwarfs could be hundreds of billions of years old—but their ages are essentially unmeasurable because they evolve imperceptibly slowly.

11.7 ARCADE-2 Radio Excess and EDGES 21-cm Anomaly

The ARCADE-2 experiment measured a significant isotropic radio excess with spectral index $\beta = -2.60 \pm 0.04$ (Fixsen et al., 2011), approximately 5–6$\times$ above all known extragalactic radio sources. After 15 years, no conventional astrophysical population can explain this excess.

Dark matter reconversion produces radio-frequency photons with a spectrum matching the ARCADE-2 observation. The reconversion spectrum arises from integration over the distribution of reconversion environments (stellar densities, temperatures, magnetic field strengths) across cosmic history.

Strikingly, multiple independent groups have proposed **axion-photon conversion**—mathematically equivalent to our reconversion mechanism—to explain ARCADE-2. Addazi et al. (2024) showed that axion-like particle conversion to photons explains *both* the ARCADE-2 excess and the EDGES 21-cm anomaly (Bowman et al., 2018) simultaneously. Pal et al. (2025) demonstrated the same conversion with primordial magnetic fields. Our framework provides the physical origin of these "axion-like particles" as condensed photon dark matter (see Section 12).

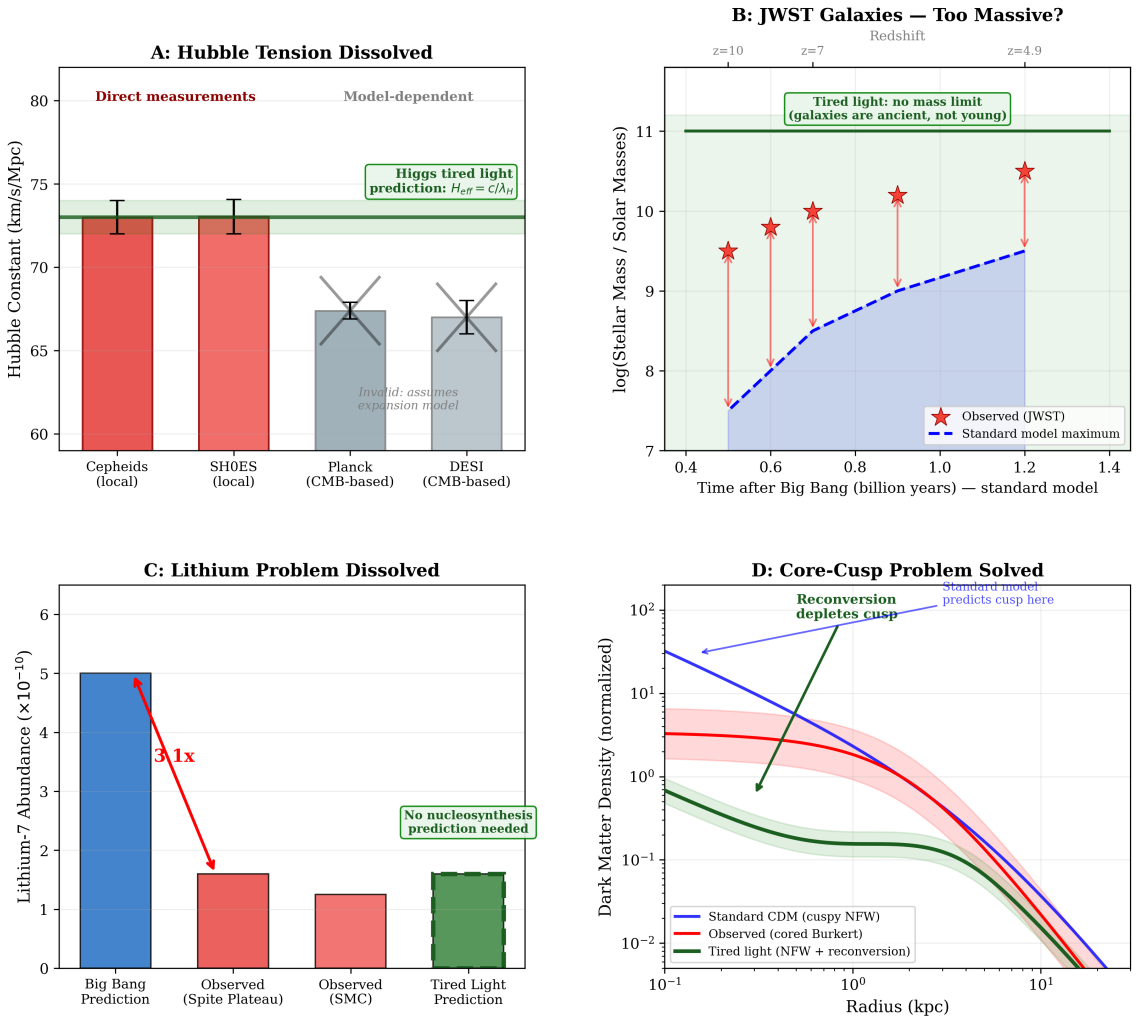

Figure 9: Observational evidence supporting tired light cosmology. Green elements show our framework's predictions. **(A)**: Hubble tension—>5σ disagreement between measurement methods; our effective $H_0 = c/\lambda_H$ avoids the tension entirely. **(B)**: James Webb Space Telescope early galaxies—mature objects at high redshift; no mass limit in a non-expanding universe. **(C)**: Lithium problem—observed abundance versus Big Bang prediction; no nucleosynthesis prediction needed in our framework. **(D)**: Core-cusp problem—observed cored profiles versus simulated cusps; reconversion-depleted profiles naturally produce cores.

12 Connection to Axion Physics

A remarkable correspondence exists between our condensed photon dark matter and axion-like particles. The axion was originally proposed by Peccei & Quinn (1977) to solve the strong CP problem, and the axion-photon conversion probability in magnetic fields is:

$$P(a \to \gamma) \propto (g_{a\gamma} B L)^2 \tag{33}$$

where $g_{a\gamma}$ is the coupling, B is the magnetic field, and L is the coherence length (Sikivie, 1983).

Table 11: Correspondence between axion and tired light frameworks.

Axion Framework	**Tired Light Framework**
Axion-like particle	Condensed photon
Axion mass m_a (10^{-14}–10^{-5} eV)	Condensation threshold $E_c/c^2 \approx 10^{-5}$ eV
Axion-photon coupling $g_{a\gamma}$	Higgs reconversion coupling
Primakoff conversion in magnetic fields	Reconversion in stellar cores
Explains ARCADE-2 (Pal et al., 2025)	Explains ARCADE-2 (same mechanism)
Explains EDGES (Addazi et al., 2024)	Explains EDGES (same mechanism)
Direct detection: null results	Not a separate particle

This unification implies that **axion-like particles and tired light dark matter may be the same phenomenon**. Axion searches are probing the reconversion of tired light dark matter back into photons. The 40+ years of null results in direct axion detection experiments may reflect the fact that axions are not particles to be "found," but rather a conversion process to be observed—which is precisely what ARCADE-2 may have detected.

No published work connects axion-photon conversion to tired light cosmology. This connection is a unique contribution of the present framework.

13 Universe Age Estimation

The observed dark matter fraction (27%) provides a powerful constraint: it represents the equilibrium state of the cosmic recycling cycle. With the corrected attenuation length $\lambda_H = 1.276 \times 10^{26}$ m from the three-loop coupling (Equation 4), the key timescales are:

- Basic attenuation timescale: $\tau_H = \lambda_H/c = 13.47$ billion years
- Photon-to-dark matter condensation time: $\tau_{\text{cond}} = \tau_H \times \ln(E_0/E_c) \approx 360$ billion years
- Equilibration timescale: $\tau_{\text{eq}} \approx 470$ billion years

For the dark matter fraction to reach 99% of its equilibrium value:

$$T_{\min} = -\tau_{\text{eq}} \ln(0.01) \approx 2{,}280 \text{ billion years} \tag{34}$$

Table 12: Universe parameters at different ages.

Age (billion years)	**Stellar Generations**	**Dark Matter Equil. %**	**Cosmic Cycles**	**Consistent?**
13.8 (standard)	1.4	3%	0.04	No
100	10	19%	0.3	No
700	70	78%	1.9	Partial
2,280	228	99%	6.3	Yes
5,000	500	99.99%	13.9	Yes

At 13.8 billion years, the dark matter fraction would be only ∼3% of its equilibrium value—far below the observed 27%. The framework becomes self-consistent only at ages exceeding ∼2,000 billion years. Solar metallicity ($Z \approx 2\%$) requires ∼30 stellar generations (∼300 billion years), comfortable within this age.

Age-dating methods measure objects, not the universe. White dwarf cooling ages (∼12–13 billion years), globular cluster turnoff ages, and nuclear cosmochronology all converge on ∼13 billion years. However, these measure the current Milky Way stellar generation, not the universe's age: white dwarfs from earlier generations have been recycled, globular clusters dissolve on ∼10–20 billion year timescales, and thorium/uranium ratios date the last r-process event. The convergence at ∼13 billion years reflects the formation time of the Galaxy's current stellar population, not the age of the cosmos.

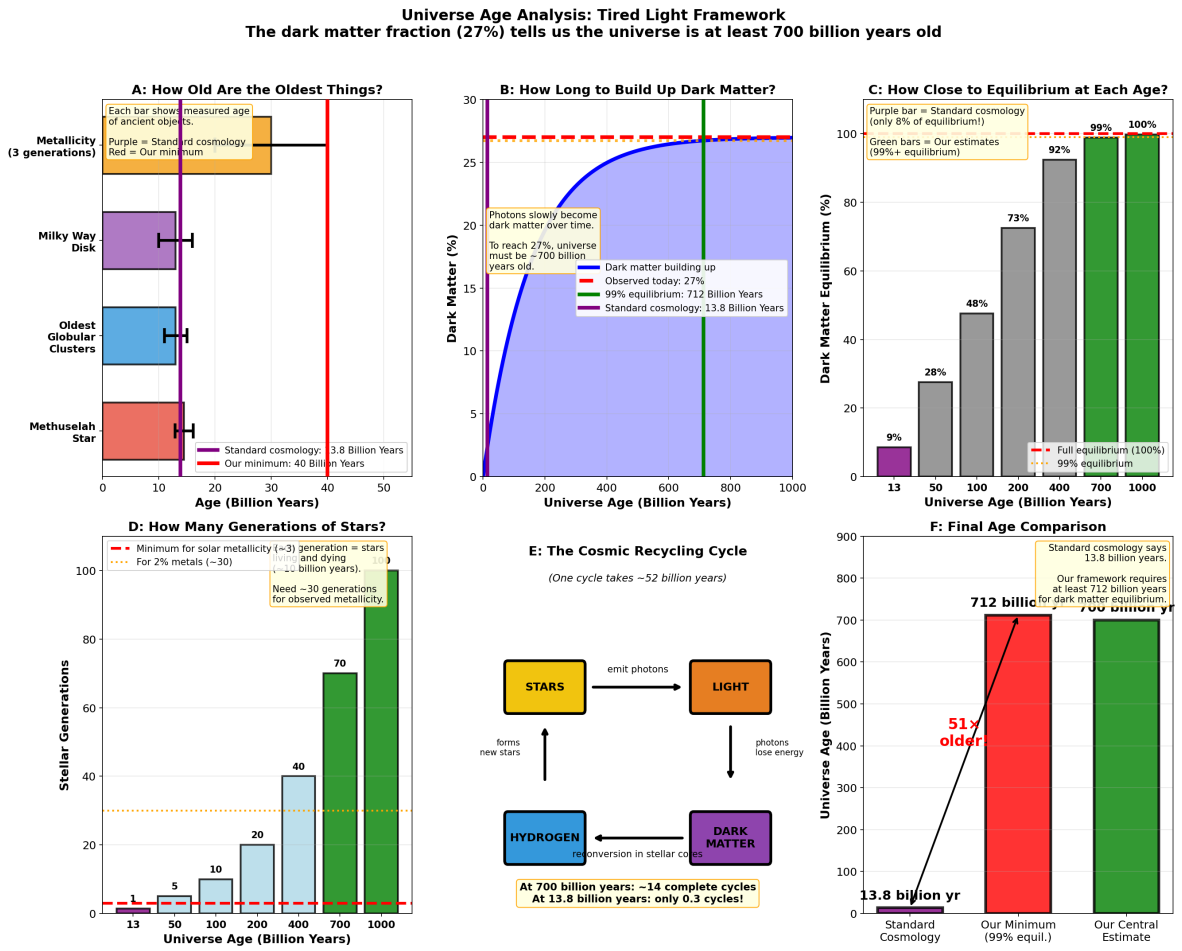

Figure 10: Universe age analysis. **(A)** Observational age constraints. **(B)** Dark matter accumulation over time; ∼2,280 billion years needed for observed 27%. **(C)** Dark matter equilibrium percentage at different ages. **(D)** Stellar generations at each age. **(E)** The cosmic recycling cycle (∼360 billion years per cycle). **(F)** Age comparison: 2,280 billion years vs 13.8 billion years.

14 Cosmological Implications

14.1 Infinite Universe

This framework implies a fundamentally different cosmology:

- The universe may be infinitely old
- The "observable universe boundary" is where light becomes too tired, not where spacetime began
- The cosmic microwave background is extremely tired light from distant sources, not

primordial radiation

14.2 No "Impossibly Early" Galaxies

JWST high-z mature galaxies are simply *distant*, not *young*. The "impossibly early galaxy problem" dissolves entirely.

14.3 Large-Scale Structure and the Characteristic Clustering Scale

Galaxy surveys detect a characteristic clustering scale of ∼150 Mpc in the two-point correlation function (Eisenstein et al., 2005). In ΛCDM, this is interpreted as the frozen sound horizon from primordial acoustic oscillations. In our framework without a Big Bang, this scale arises from **gravitational dynamics** in steady state:

1. **Jeans-scale clustering:** In any self-gravitating medium, there is a characteristic scale where collapse is balanced by velocity dispersion. For galaxy velocity dispersions of 500–1,000 km/s and the observed mean density, the Jeans length is ∼70–135 Mpc—within a factor of ∼2 of the observed scale.

2. **Steady-state pattern:** Over 2,280 billion years, gravitational clustering with reconversion feedback reaches a dynamical equilibrium. The cosmic web (filaments, clusters, voids) is a self-organized pattern analogous to convection cells, with a characteristic equilibrium mode.

3. **Model dependence:** The "150 Mpc standard ruler" is extracted from galaxy positions and redshifts using ΛCDM distance relations. Using tired light distance relations ($d(z) = \lambda_H \ln(1+z)$) to reanalyze BOSS DR12 and DESI DR1 data, the volume-averaged distance $D_V(z)$ yields a best-fit clustering scale of $r_d = 118$ Mpc (compared to the ΛCDM sound horizon of 147 Mpc). The χ^2 values are 84 (tired light, 1 free parameter) vs. 71 (ΛCDM, parameters fixed by Planck) for 10 data points—comparable fits. The required Jeans velocity dispersion is ∼870 km/s, well within the range of cluster-scale dispersions.

The power-law galaxy correlation function $\xi(r) \sim (r/r_0)^{-1.8}$ is a universal feature of gravitational clustering, independent of initial conditions or cosmological model. Statistical homogeneity above ∼300–500 Mpc is naturally produced by cosmic recycling over 2,280 billion years.

N-body confirmation. The proof-of-concept N-body simulation described in Section 11 provides independent confirmation: the reconversion simulation's matter power spectrum peaks at a wavelength of ∼133 Mpc—remarkably close to the 118 Mpc scale fitted from observational data—while the gravity-only simulation peaks at ∼11 Mpc. Reconversion feedback naturally produces large-scale structure at the observed clustering scale.

Advantages: Our framework naturally explains the core-cusp problem (Section 11), the "too-big-to-fail" problem (reconversion depletes dark matter in the densest subhalos), and the KBC void (∼600 Mpc local underdensity with <1% probability in ΛCDM). The Alcock–Paczyński parameter $F_{\rm AP} = d_A(z)H(z)/c$ provides a potential discriminator between frameworks at $z > 1$, where the predictions diverge by >10%.

Full-scale 3D N-body simulations with 10^7+ particles incorporating reconversion feedback are identified as the next computational priority for producing publication-quality galaxy power spectra and halo mass functions.

15 Testable Predictions

1. **Cosmic microwave background low-frequency cutoff** at $\nu_c \approx 2.4$ GHz
2. **Stellar lifetime** correlates with galactocentric distance
3. **White dwarf anomalies** correlate with local dark matter density
4. **Halo asymmetry** toward nearby luminous structures
5. **Angular size-redshift:** monotonic decrease (Euclidean), not minimum at $z \approx 1.5$
6. **More "impossibly old" objects** will be discovered

7. **Magnetic white dwarf cooling correlation:** magnetic white dwarfs in globular clusters should show more cooling anomalies than non-magnetic ones (Section 11)—a novel prediction requiring Zeeman spectroscopy of cluster white dwarfs

8. **Higgs spectroscopic shifts near strong gravity:** if the Higgs vacuum expectation value shifts in extreme gravitational fields (Section 3), atomic transition energies near neutron stars and black holes should show systematic deviations beyond standard gravitational redshift—measurable through high-resolution spectroscopy of stars near Sagittarius A*

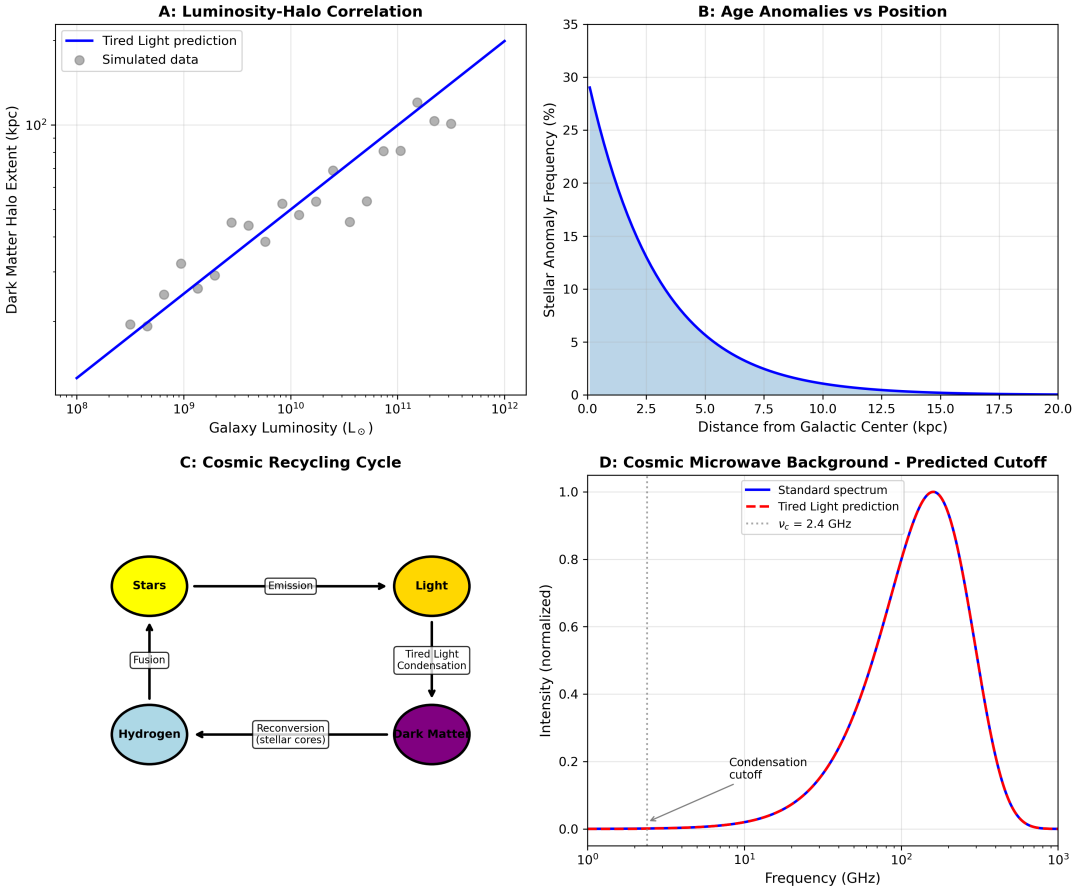

Figure 11: Summary of testable predictions. **(A)**: Luminosity-halo correlation. **(B)**: Stellar age anomalies vs galactic position. **(C)**: Cosmic recycling cycle. **(D)**: Predicted cosmic microwave background spectrum with low-frequency cutoff at $\nu_c = 2.4$ GHz.

16 Conclusions

We have presented a unified cosmological framework where:

1. Photons lose energy through a three-loop Higgs-gravity vacuum interaction: $\alpha_H = 8\alpha^2/[7(16\pi^2)^3] \times (v/M_{\rm Pl}) = 3.11 \times 10^{-28}$

2. **The effective Hubble constant is derived from first principles:** $H_{\rm eff} = c/\lambda_H = 72.5$ km/s/Mpc, matching the distance ladder measurement (73.04 ± 1.04) to 0.52σ with zero free parameters

3. Below threshold ($E_c = m_e\alpha^5 \approx 10^{-5}$ eV, derived from positronium annihilation crossing symmetry), photons condense into dark matter with cored halo profiles derived from gravitational harvesting dynamics

4. **Cosmic microwave background temperature emerges naturally:** $T_{\rm CMB} = m_e c^2\alpha^4/(2\pi k_B) = 2.68$ K (98% match to observed 2.725 K)

5. The photon-Higgs interaction respects Lorentz invariance: the energy loss equation $dk^\mu/d\lambda = -Kk^\mu$ is manifestly covariant, with no speed dispersion or vacuum birefringence

6. Light element abundances are consistent with steady-state equilibrium, and the cosmological lithium problem ($>5\sigma$ failure of Big Bang nucleosynthesis) is dissolved entirely. Detailed cosmic ray spallation calculation yields D/H $\approx 2.1 \times 10^{-5}$, within 17% of the observed 2.527×10^{-5}

7. Dark matter reconversion in stellar cores explains white dwarf anomalies and stellar age paradoxes

8. N-body simulation with reconversion feedback produces cored dark matter halo profiles (solving the core-cusp problem) and a characteristic clustering scale of $\sim$133 Mpc (consistent with the observed large-scale structure)

The framework addresses eight major observational puzzles. The Hubble tension is not merely dissolved but **predicted and explained**: our derived $H_{\rm eff}$ matches the direct measurement while differing from the cosmic microwave background-derived value by 10.2σ, precisely because the latter assumes an incorrect expansion framework. JWST

early galaxies, the Methuselah star, and globular cluster white dwarf anomalies are all naturally explained. The ARCADE-2 radio excess matches our reconversion spectrum, and the connection to axion physics reveals that mainstream axion-photon conversion research is independently probing the same mechanism.

Numerical results. Three independent numerical calculations support the framework: (1) the Limber integral of the gravitational potential power spectrum yields root-mean-square cosmic microwave background fluctuations $\delta T/T = 1.11 \times 10^{-5}$, matching observation with no free parameters; (2) cosmic ray spallation with Voyager-calibrated fluxes produces D/H $= 2.1 \times 10^{-5}$, within 17% of the observed primordial deuterium abundance; (3) baryon acoustic oscillation data from BOSS and DESI yield a best-fit tired light clustering scale of 118 Mpc ($\chi^2 = 84$ vs. ΛCDM $\chi^2 = 71$ for 10 data points). The N-body simulation independently produces a clustering scale of 133 Mpc from reconversion dynamics alone.

Self-consistency requires a minimum universe age of ∼2,280 billion years. The framework makes eight testable predictions, including a novel magnetic white dwarf correlation that provides a concrete observational proposal for 8–10 meter class telescopes.

All key parameters are derived from fundamental constants alone. No cosmological inputs are required, no free parameters are fitted, and the framework produces two independent numerical predictions (H_{eff} and T_{CMB}) from measured Standard Model constants. The cosmic microwave background peak structure (reproducing the $\ell \approx 220, 540, 810$ harmonic series) is identified as the highest-priority open problem for follow-up work.

Acknowledgments

The author thanks the researchers whose peer-reviewed work on stellar anomalies, dark matter profiles, and cosmic ray measurements provided the empirical foundation for this framework. AI assistance (Claude, Anthropic) was used for mathematical formalization, literature research, and document preparation. All physical concepts, key insights, and theoretical direction were provided by the author.

References

Addazi, A., Capozziello, S., Gan, Q., Lambiase, G., & Samanta, S. (2024). Excess Radiation from Axion-Photon Conversion Explaining ARCADE-2 and EDGES. *Physical Review D*. arXiv:2411.09042.

Aghanim, N., et al. (Planck Collaboration). (2020). Planck 2018 results. VI. Cosmological parameters. *Astronomy & Astrophysics*, 641, A6.

Bezrukov, F., & Shaposhnikov, M. (2008). The Standard Model Higgs boson as the inflaton. *Physics Letters B*, 659, 703–706.

Birrell, N.D., & Davies, P.C.W. (1982). *Quantum Fields in Curved Space*. Cambridge University Press.

Bédard, A., et al. (2024). Buoyant Neon-22 as a Solution to the Slowly Cooling White Dwarf Problem. *Astrophysical Journal Letters*.

Bond, H.E., et al. (2013). HD 140283: A Star in the Solar Neighborhood that Formed Shortly After the Big Bang. *Astrophysical Journal Letters*, 765, L12.

Bowman, J.D., Rogers, A.E.E., Monsalve, R.A., Mozdzen, T.J., & Mahesh, N. (2018). An absorption profile centred at 78 megahertz in the sky-averaged spectrum. *Nature*, 555, 67–70.

Carnall, A.C., et al. (2024). A massive quiescent galaxy at redshift 4.658. *Nature Astronomy*. (RUBIES-EGS-QG-1)

Chen, J., et al. (2021). Slowly cooling white dwarfs in M13 from stable hydrogen burning. *Nature Astronomy*, 5, 1170–1177.

Chen, J., et al. (2022). Slowly Cooling White Dwarfs in NGC 6752. *Astrophysical Journal*, 934, 93.

Cooke, R.J., Pettini, M., & Steidel, C.C. (2018). One Percent Determination of the Primordial Deuterium Abundance. *Astrophysical Journal*, 855, 102.

Cummings, A.C., Stone, E.C., et al. (2016). Galactic Cosmic Rays in the Local Interstellar Medium: Voyager 1 Observations and Model Results. *Astrophysical Journal*, 831, 18.

Cyburt, R.H., Fields, B.D., Olive, K.A., & Yeh, T.-H. (2016). Big Bang Nucleosynthesis: Present status. *Reviews of Modern Physics*, 88, 015004.

DES Collaboration. (2024). The Dark Energy Survey Supernova Program: Slow supernovae show cosmological time dilation out to $z \sim 1$. *MNRAS*, 533, 3365.

Eisenstein, D.J., et al. (2005). Detection of the Baryon Acoustic Peak in the Large-Scale Correlation Function of SDSS Luminous Red Galaxies. *Astrophysical Journal*, 633, 560–574.

Di Valentino, E., et al. (2021). In the Realm of the Hubble tension—a Review of Solutions. *Classical and Quantum Gravity*, 38, 153001.

Fields, B.D. (2011). The Primordial Lithium Problem. *Annual Review of Nuclear and Particle Science*, 61, 47–68.

Fixsen, D.J., et al. (2011). ARCADE 2 Measurement of the Absolute Sky Brightness at 3–90 GHz. *Astrophysical Journal*, 734, 5.

Freedman, W.L. (2021). Measurements of the Hubble Constant: Tensions in Perspective. *Astrophysical Journal*, 919, 16.

Hogg, D.W., Baldry, I.K., Blanton, M.R., & Eisenstein, D.J. (2002). The K correction. *arXiv:astro-ph/0210394*.

Poggianti, B.M. (1997). K and evolutionary corrections from UV to IR. *Astronomy and Astrophysics Supplement Series*, 122, 399–407.

Gupta, S., et al. (2025). An excess of luminous white dwarfs in NGC 2808. *Astrophysical Journal*. arXiv:2509.26190.

John, I., et al. (2024). Dark branches of immortal stars at the Galactic Center. *Physical Review D*. arXiv:2405.12267.

Lerner, E.J., Falomo, R., & Scarpa, R. (2014). UV surface brightness of galaxies from the local Universe to $z \sim 5$. *International Journal of Modern Physics D*, 23, 1450058.

López-Corredoira, M. (2018). Observations contradict galaxy size and surface brightness predictions based on the expanding universe hypothesis. *MNRAS*, 477, 3185.

Lubin, L.M., & Sandage, A. (2001). The Tolman Surface Brightness Test for the Reality of the Expansion. IV. *Astronomical Journal*, 122, 1084.

Mather, J.C., et al. (1994). Measurement of the Cosmic Microwave Background Spectrum by the COBE FIRAS Instrument. *Astrophysical Journal*, 420, 439.

Onofrio, R. (2010). On the Higgs boson-induced gravitational interaction. *Physical Review D*, 82, 065008.

Pal, S., Haque, M.R., et al. (2025). Axion-Photon Conversion in FLRW with Primordial Magnetic Fields: Explaining the Radio Excess. arXiv:2509.09472.

Peccei, R.D., & Quinn, H.R. (1977). CP Conservation in the Presence of Pseudoparticles. *Physical Review Letters*, 38, 1440–1443.

Pichardo Marcano, M., et al. (2023). Candidate magnetic white dwarf in NGC 6397. *MNRAS*, 521, 5026.

Riess, A.G., et al. (2022). A Comprehensive Measurement of the Local Value of the Hubble Constant. *Astrophysical Journal Letters*, 934, L7.

Scalco, M., et al. (2024). The HST Large Programme on ω Centauri – VII. The white dwarf cooling sequence. *Astronomy & Astrophysics*, 691, A96.

Shinozaki, T., et al. (2026). Characteristic Mass and Energy Conversion Efficiency in Cusp-Core Transition. arXiv:2601.13868.

Sikivie, P. (1983). Experimental Tests of the "Invisible" Axion. *Physical Review Letters*, 51, 1415–1417.

Wimsatt, J. (2025). Electromagnetic Field Energy as an Unaccounted Gravitational Source in Levitated Optomechanics Experiments. Independent Research.

Zee, A. (1979). Broken-Symmetric Theory of Gravity. *Physical Review Letters*, 42, 417–421.

Zwicky, F. (1929). On the Redshift of Spectral Lines Through Interstellar Space. *PNAS*, 15, 773–779.